Lithium adsorption on MgO(100) and its defects: Charge transfer, structure, and energetics

J. A. Farmer, N. Ruzycki, J. F. Zhu, and Charles T. Campbell*
Department of Chemistry, University of Washington, Seattle, Washington 98195-1700, USA
(Received 3 March 2009; revised manuscript received 21 May 2009; published 15 July 2009)

The adsorption energetics and growth of lithium vapor on MgO(100) at 300 K was studied using microcalorimetry, in combination with low-energy electron diffraction (LEED), low-energy ion scattering (ISS), Auger electron spectroscopy (AES), and work-function measurements. The MgO(100) samples were films of ~4 nm thickness grown on a Mo(100) single crystal. The initial sticking probability of lithium was ~0.97, reaching unity by 0.5 monolayer (ML). The AES and ISS signals vary with Li coverage up to 3 ML as expected if the Li atoms stay within the layer where they initially hit (i.e., with no interlayer transport). Initially, lithium adsorbs strongly at the intrinsic surface defects and as two-dimensional (2D) lithium clusters, with a heat of adsorption of 260 kJ/mol. The heat approaches the heat of sublimation of bulk Li (159 kJ/mol) by 0.4 ML, due to the growth of 2D and then three-dimensional (3D) Li islands. Argon-ion sputtering of the surface increases the defect density and the probability for adsorbing Li to find a defect, and thus the heat of adsorption at low coverages. When defects only are being populated, Li exhibits a heat of adsorption of 410 kJ/mol. Comparing heats with recent density functional theory (DFT) calculations suggests that the defect sites are under-coordinated O atoms at steps or kinks, or related structures at dislocations. The work function decreases by ~1.8 eV within the first 0.5 ML and then increases to near the value of bulk Li(solid), ~2.6 eV, by 3 ML. These results support recent DFT calculations predicting stronger electron transfer from Li to the MgO when at steps and kinks than at terraces, and decreasing charge transfer as 2D Li clusters grow. The work function starts to increase when the growth mode becomes dominated by growth of 3D Li(solid). In spite of a large amount of electron transfer from Li to MgO, Li adatoms have attractive interactions that lead to 2D clustering. For 1-nm-thick MgO films, the heat of adsorption was higher by 60–20 kJ/mol than for 4 nm films in the entire range from 0 to 0.7 ML, where adsorption in the first layer dominates.

DOI: 10.1103/PhysRevB.80.035418 PACS number(s): 68.43.−h, 68.35.Md, 05.70.Np, 07.20.Fw

I. INTRODUCTION

The production of chemicals from natural gas is a potential application of heterogeneous catalysts that can help to offset or ameliorate the environmental impact of fossil fuel usage. The partial oxidation of methane to higher alkenes (olefins, chemical feedstocks for alcohol, and aldehyde production) is under investigation and lithium-promoted magnesium oxide was found to catalyze such reactions. Many years of fundamental research has been devoted to studying the catalytic mechanism and performance of this catalyst to enable its use in technological applications.[1–3] Catalytic investigations found that lithium reacts with oxygen sites on MgO forming ionic species that can abstract hydrogen from alkanes.[3]

Surface science investigations of alkali metal adsorption (K, Na, and Cs) on MgO(100) observed that alkali atoms bind weakly to terraces, with surface defect sites acting as nucleation centers for three-dimensional (3D) particle growth.[4–6] Huang *et al.*[6] observed partial wetting of MgO(100) by *K* at low coverages and then a switch to 3D particle growth. Brause *et al.*[5] observed a specific Cs medium energy ion scattering peak at low coverage for Cs on MgO(100) (<0.1 ML), and assigned it to Cs adsorption at steps or kinks on the MgO(100) surface. Kendelewicz *et al.*[4] studied Na adsorption on MgO(100) and interpret their data as Na adsorbing at defect sites, which act as nucleation centers. These studies also observed electron-density transfer from the alkali metal to the metal oxide surface. Lithium adsorbates on MgO(100) were found to follow similar growth patterns, and were found to exhibit charge transfer characteristics on MgO(100) by electron paramagnetic resonance and by theoretical density-functional calculations.[7–10]

We report here single-crystal adsorption microcalorimetric measurements, supported with Auger electron spectroscopy (AES), low-energy ion scattering (ISS), and work-function measurements of Li adsorption on MgO(100) thin films (1 and 4 nm thick) grown on Mo(100), and on ion-sputtered MgO(100) surfaces. The ISS measurements and some of the microcalorimetry measurements presented here for Li adsorption were reported elsewhere, see Ref. 11, in an article that compared and contrasted those measurements with our earlier results for Ca adsorption on MgO(100).[12] In that article, it was shown that combining microcalorimetric measurements with DFT and kinetic modeling provides a way to learn about the nature of oxide surface defects, their concentrations, and the probability distributions of local defect concentration across the surface. Here we present AES measurements that prove the structural model proposed previously based on ISS and heat of adsorption measurements, and we present work-function measurements that probe the electronic aspects of Li binding to MgO(100). We correlate these structural and electronic measurements with microcalorimetric adsorption energy measurements. Work function versus metal coverage has not been measured previously for such a well-characterized alkali-on-oxide system where step-site adsorption was known to play such an important role as here and where adsorption energy measurements could identify the strength of bonding at defects. The rich coverage dependence of the work function is unusual, and careful analysis of the results, when compared with recent DFT cal-

culations of charge transfer and bonding energy at the same types of defect and terrace sites,[11,13] and our heat of adsorption measurements, provide unique understanding of alkali-induced work function changes on oxide surfaces and alkali-oxide bonding that is of generic interest. Finally, we present measurements that reveal how the heats of adsorption of Li on thin MgO(100) films depend on film thickness.

A key emphasis in this paper is the nature of the binding of Li to defect sites on the MgO(100) surface. For MgO(100) films grown on Mo(100), as we do here, these defect sites have been extensively studied.[14–21] In the range of MgO film thicknesses from 1.5 to 4 nm, scanning tunnel microscope (STM) studies show a similar film morphology, with the strongly predominant defects being extended defects similar to step edges and associated kink sites, although they appear to also include domain boundaries and screw dislocations that probably arise from the lattice mismatch between Mo(100) and MgO(100).[14–17] These edges offer under coordinated O sites similar to those at step and kink sites. Since the DFT calculations of Li adsorption to which we can compare were only done on step and kink sites and not on such edges,[11,13] we discuss our results here mainly as if the defects are steps and kink sites only, but we wish to emphasize that these comparisons might be more appropriate if also made to their analogous sites at domain boundaries and dislocations instead. We find here that Li binds rather cationically to such defects. In that respect, is interesting to note that these step-like defects have been observed to have a very high-local work function,[15] which will facilitate stronger bonds to Li in its cationic bonding, consistent with what we observe here by calorimetry and work function.

II. EXPERIMENTAL

The microcalorimetry experiment and apparatus has been described in detail previously.[22] The calorimeter was housed in an ultrahigh vacuum chamber, with a base pressure of $\sim 2\times 10^{-10}$ mbar (rising to $\sim 1\times 10^{-9}$ mbar, which was mainly H_2, during Li deposition). It was equipped with low-energy electron diffraction (LEED), AES, and ISS, a quadrupole mass spectrometer (QMS) and a quartz-crystal microbalance (QCM).

The calorimeter consists of a pulsed metal atom beam and a pyroelectric polymer (PVDF) ribbon, as described elsewhere.[22] Different from this previous calorimeter, here we used a so-called double PVDF ribbon assembly, whereby a back ribbon of opposite polarity was placed against the front ribbon to serve as a reference signal which is subtracted from the signal on the ribbon contacting the sample. This eliminates some of the noise signal that originates from the ribbon's piezoelectric response to mechanical vibrations, similar to the double ribbon assembly as described previously,[23] but without the Kapton ribbon between the PVDF ribbons. The voltage output (heat signal) is calibrated by using light pulses of known energy as described previously.[22] The typical calorimeter sensitivity was 120–160 V/J (volts at peak maximum per adsorbed joule in the pulse) for these experiments. This is higher than previous values (typically 10–100 V/J),[22] which we attribute to the better thermal/mechanical contact between the detector and the sample due to the additional force provided by the back ribbon.

A 4 mm diameter, chopped Li atom beam is produced from a high-temperature effusion cell, as described previously.[22] The metal atom beam is chopped to provide 100 ms pulses containing 0.006–0.01 monolayer (ML) Li (purchased from Alfa Aesar with 99% purity) every two seconds. 1 ML of Li was defined throughout as 1.12×10^{15} atoms/cm^2, which is the MgO(100) unit-cell density. The absolute beam flux is measured by using a calibrated QCM. The sticking probability is measured by a modified King-Wells method, using a line-of-sight QMS at the magic angle[24] to measure the fraction of metal atoms which strike the surface but do not adsorb. The mass spectrometer signal was calibrated by measuring the integrated desorption signal from a known amount of Li reflected from a hot Ta foil (750 to 950 K), which was located at the same position as the sample and corrected for average velocity.

The typical operating temperature of the effusion cell was $\sim$775 K, which generated some thermal radiation that impinged on the sample and also was detected by the calorimeter (0.03 μJ/pulse or $\sim$17 kJ of absorbed radiation per mole of dosed Li). This radiation was measured by blocking the metal beam with a BaF_2 window, which blocked the metal atoms from impinging onto the surface of the sample but passed a known fraction of the radiation, which was subtracted from the total measured signal. The radiation contribution can change if the sample's optical reflectivity changes due to metal adsorption. We measured the sample reflectivity as described in Ref. 25 and in the coverage range of interest (0–5 ML of Li) the reflectivity remained constant at 57%.

To convert these measured internal energy changes into standard enthalpy changes at the sample temperature (300 K), the excess translational energy of the metal gas atoms at the oven temperature, above that for a 300 K Maxwell-Boltzmann distribution ($\sim$0.05 μJ/pulse), is subtracted, and a small pressure-volume work term (RT per mole) is added, as described elsewhere.[22] The corrected enthalpy of adsorption is thus the standard molar enthalpy of adsorption at 300 K, which at high coverage, where the atoms are adding to bulk-like sites, can be compared directly to the standard heat of sublimation of the metal. The measured heats are expressed as the enthalpy of adsorption on a "per mole of adsorbed Li" basis by correcting for the sticking probability.[22]

The preparation and characterization of the 1 μm-thick Mo(100) single-crystal sample and the MgO(100) thin films were described elsewhere.[26] The cleanliness and order of the Mo(100) and MgO(100) surfaces were characterized using AES and LEED. The MgO(100) films were grown to thicknesses of 1 and 4 nm, measured using AES and the mean-free path of Mo electrons. AES experiments were carried out using 1.6 keV electrons from a PHI LEED system (15–120) and a Leybold-Heraeus EA11 hemispherical energy analyzer. ISS experiments were carried out using He^+ ions with 1 keV primary energy using a focused ion gun (Leybold-Heraeus IQE 12/38). Work function changes ($\Delta\Phi$) were measured by the shifts in the low-energy onset of the secondary electrons in the Auger spectra with the sample negatively biased, using a very low-pass energy ($\Delta E=3$ eV) for high resolution, and a very low electron beam current.

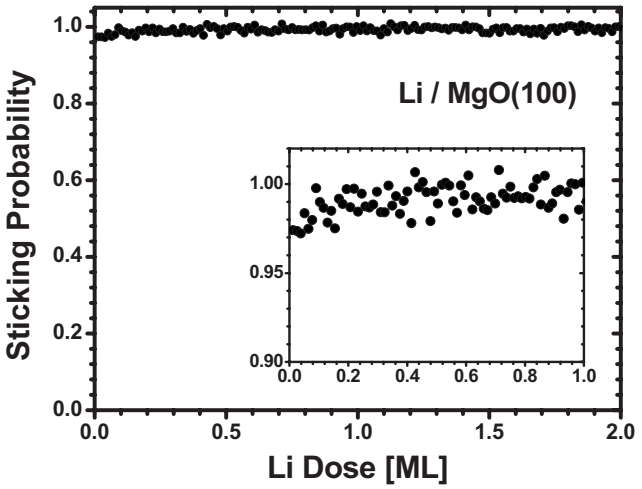

FIG. 1. The sticking probability of Li onto MgO(100) at room temperature as a function of the total amount of Li dosed.

III. RESULTS AND DISCUSSION

A. Sticking probability

The sticking probability of Li gas onto a MgO(100) surface at 300 K as a function of coverage is shown in Fig. 1. The gas here is at the source temperature, 775 K. The sticking probability is very high. It starts at ~0.97 and increases to unity by ~0.5 ML and thereafter remains constant.

B. Li growth morphology

The growth mode of Li on MgO(100) at 300 K was investigated using LEED, AES, and ISS. At Li coverages of 0.25, 0.5, 0.75, 1, 1.5, 2, and 5 ML, the surface was checked for ordering by LEED. No new LEED spots due to the adsorption of Li were seen, with only an increasingly diffuse background for the MgO(100) LEED spots.

Figure 2 shows the AES results for the growth of Li on MgO(100) at 300 K. The open circles represent the integrated intensity of the Li Auger peak at 43 eV, normalized to the signal from a thick, bulk-like Li film on MgO(100) (>15 ML), as a function of Li coverage at 300 K. The closed circles show the integrated intensity of the Mg Auger peak at 32 eV, normalized to the Mg signal from pristine MgO(100).

High noise levels are apparent in Fig. 2 due to the overlap of the large and changing low-energy secondary electron background with the Li and Mg peaks. Due to Li-induced work function changes, this baseline changes with Li coverage, making integration of these peak areas less precise.

With increasing Li coverage, the normalized AES intensity for Li approaches unity and that for Mg approaches zero. The gray and black lines show the calculated results for a layer-by-layer growth model.[27] Above ~1 ML, the signal for Mg stays above this model and changes more slowly with Li coverage. The Mg data above 1 ML are better fit by the "no down-step/up-step model" shown in Fig. 2, wherein the Li atoms are assumed to stay in the layer into which they initially land, without any diffusion between layers (no down stepping to the layer below nor up stepping to the layer above). That is, the fraction of incoming Li atoms that add to layer N at any time is equal to the fraction of the surface that has vacant sites in layer N-1. This model was propagated by a simple iterative computational method using incremental increases in Li coverage. It gave the same results as calculated using the equations in Ref. 28 if one uses in their equations the full expression for the transmission coefficient [i.e., the probability that an electron escape through a single atomic layer, $\exp(-d/(\lambda \cos \theta))$, where d is the monolayer thickness, λ is the inelastic mean-free path, and θ is the detection angle] instead of its less accurate approximation as the first term in its Taylor series expansion used in Ref. 28. While this model includes no explicit assumptions about diffusion within layers, the model is physically reasonable only when there is at least limited transport within each layer (but not between layers) that allows significant two-dimensional (2D) clustering, since atoms which land on top of monomers and dimers would rapidly move to the layer below, but the same would not happen on larger clusters (according to DFT calculations).[11] As described below, the measured heats of adsorption indicate a high probability of populating defects at very low coverages, which also requires rapid diffusion across MgO(100) terraces (i.e., within the first layer diffusion is rapid, but diffusion between layers is kinetically forbidden). This is consistent with DFT calculations.[11] This model fits the Mg data well up to ~2 ML coverage, above which the data deviate above this model slightly, which could be explained by including some limited Li atom up stepping, perhaps driven by the greater stability of larger Li(solid) particles. Within the noise of the AES measurement, this same growth mode was observed on both 1 and 4-nm-thick MgO(100) films.

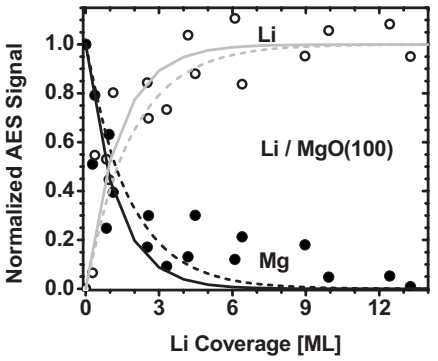

FIG. 2. The integrated Li (○) and Mg (●) AES intensities normalized to bulk Li and the clean MgO(100) surface, respectively, versus coverage for the room temperature growth of Li on a thin MgO(100) film grown on Mo(100). The solid curves correspond to what is expected if the Li film grows in a layer-by-layer manner. Dashed curves correspond to what is expected in the "No down-step/up-step model," wherein diffusion between layers is kinetically forbidden (see text). The inelastic mean-free path used for calculating the curves was 0.43 nm for Mg and 0.47 nm for Li, obtained from Ref. 67, and the detection angle was 45°. The definition of one ML (1.12×10^{15} atoms/cm^2) and the bulk density of Li(solid) give the ML thickness of 0.25 nm used here.

Distinguishing these two models on the basis of the Li AES data alone is not reliable, since it is complicated by the fact that the normalization of the Li signal to 1.0 could be too

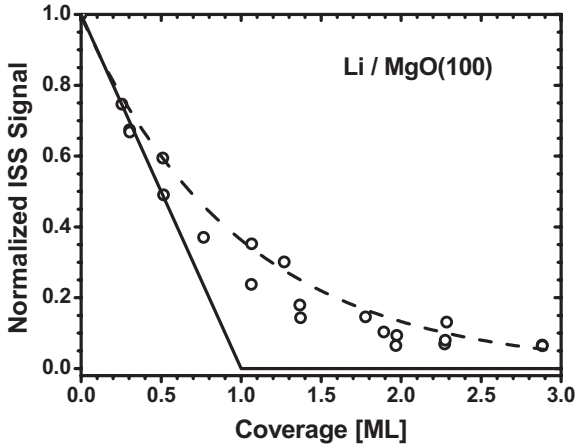

FIG. 3. Evolution of the normalized Mg (○) ISS signal as a function of Li coverage on a thin MgO(100) film grown on Mo(100) at room temperature. The solid curve shows the ISS signal for a layer-by-layer growth. The dashed curve shows a fit to the data using the no down-step/up-step model, whereby Li atoms stick in the layer in which they hit, with no diffusion between layers.

high by 10% (due to an inability to reach a truly "bulk-like" Li signal at high Li coverage).

The growth mode was further characterized by monitoring the Mg substrate signal using He^+ ISS. This provides more direct evidence on the growth mode at low coverage, due to the greater surface sensitivity of ISS, and the simplicity of the spectra (only Mg and O peaks are visible). Figure 3 shows the integrated ISS intensity of the Mg peak normalized to the clean MgO(100) Mg peak, as a function of Li coverage at 300 K. To minimize surface damage during ISS measurements the spectra were acquired over a small kinetic energy range. In addition, experiments were performed with larger coverage increments, which yielded results that overlapped the results of the longer experiments. This indicated that beam damage did not impact the result of the growth measurement within the precision of the ISS experiment.

The ISS measurement shows that the Mg signal decays nearly linearly with Li coverage to ~0.5 ML, followed by a slower decrease in intensity until the signal reaches <0.1 at ~2 ML. The solid line indicates the expected growth behavior for layer-by-layer growth, which decays too quickly compared to the data. The exponential fit to the data, plotted as a dashed line, is the result expected for the same "no down-step/up-step model" that fit the AES data well below 2 ML, which assumes that interlayer Li transport is prohibited. Within this model, if we define y as the fraction of free sites in layer 1, then the probability that an incoming Li atom lands (and stays) in layer 1 is y. If we define θ as the total Li coverage (in monolayers), then $dy/d\theta=-y$, which integrates to give $y=\exp(-\theta)$. The fit to the data using this model is nearly within the scatter of the data and certainly better than the layer-by-layer model. Within the noise of the ISS measurements, this same growth mode was observed on 1 and 4-nm-thick MgO(100) films.

C. Work function measurements

The measured work function (WF) of the pristine MgO(100) thin film was 1.1 eV below the clean Mo(100) value, which has a work function of ~4.4 eV (4.53,[29] 4.3,[30] and 4.40 eV).[31] The difference between the observed change and the Mo(100) work function sets the MgO(100) value to ~3.3 eV. Other experimental values for the WF of clean MgO(100) thin films vary widely between and within groups, and have been reported to be: 3.25,[32] 2.7,[33] 3.55,[34] and 3.9 eV.[12] This highlights the poor reproducibility of work functions for thin films of insulating oxides. For a discussion on the lack of reproducibility of oxide WF values, see also Ref. 12 and 35.

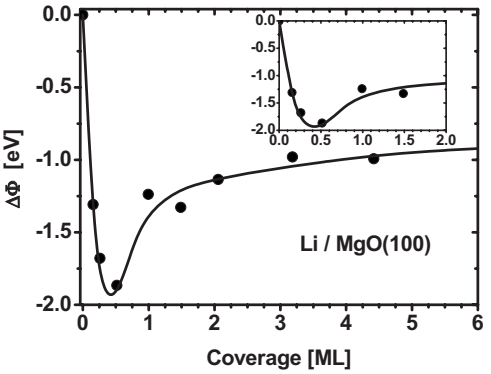

FIG. 4. The change in the work function versus Li coverage on MgO(100). The line is a guide to the eye. The inset shows the low coverage region.

Figure 4 shows the change in the MgO(100) work function versus Li coverage. Upon adsorption of Li, the work function decreased rapidly to a minimum of ~1.9 eV below that for the starting MgO by 0.5 ML. Thereafter the WF increased rapidly by ~0.7 eV by 2 ML. At the high-coverage limit (~10 ML of Li, not shown), the work function increased by ~1.2 eV from the minimum or a net decrease of ~0.7 eV with respect to the starting MgO(100) film. This sets the final work function for 10 ML of Li at ~2.6 eV. This is within 0.1 eV of the average of reported measurements of the work function of bulk Li(solid) surfaces, which range between 2.3 and 3.1 eV with an average of 2.7 eV.[36–42]

One can evaluate this coverage dependence of the work function change using the Helmholtz equation, whereby the slope at any coverage gives the dipole moment associated with adsorption of a differential amount of adsorbate.[43] The initial slope of −7.0 to −8.4 eV/ML gives an initial dipole moment of 1.7–2.0 Debye per Li atom—surface complex. This is consistent with a large extent of charge transfer or polarization (movement of electron density from Li toward the MgO). Both EPR and DFT studies of alkali metals on MgO have observed such charge transfer and/or polarization of alkali adatoms and small clusters.[7–9,44,45] One recent calculation of Li adatoms on MgO(100) surfaces was interpreted as only polarization, with no evidence for real charge transfer.[10] However, the most recent DFT slab calculations of Li on MgO(100) by Xu and Henkelman[13] concluded a transfer of 0.35 electron to MgO for Li on terraces, 0.75 electron for Li on steps, and 0.87 electron for Li on kinks. Since kinks and steps are mainly populated initially (see below), these last DFT results seem most appropriate to explain the large initial slope seen here. At step sites, the calculated charge

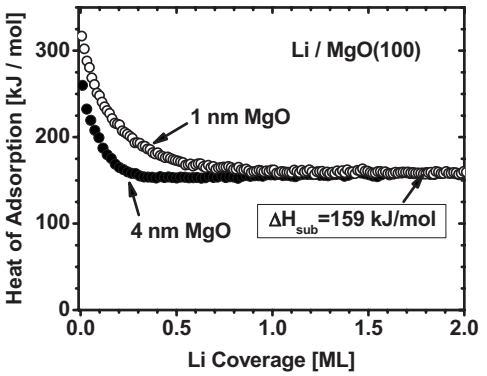

FIG. 5. The heat of adsorption versus Li coverage at room temperature on (●) a 4-nm-thick MgO(100) film and on (○) a 1–nm-thick MgO(100) film. Each data point is due to a pulse of 0.006–0.01 ML of Li (pulsed at 1/2 Hertz), and is the average of four experimental runs. 1 ML is defined as 1.12×10^{15} atoms/cm^2, which is the MgO(100) unit-cell density.

lost from the Li atom goes to the four nearest O atoms, three of which are below it and thus give downward-pointing dipoles. Interestingly, those DFT results show that the Li adatoms on terraces and defects are still strongly attracted to each other on MgO(100), in spite of these large charges.

The slope of the work function decreases until it reaches a minimum and then the work function increases above ~0.5 ML. This indicates a decrease in the extent of this ionic bonding as the dominant adsorption mode shifts, first from bonding at defects to terrace sites at the edge of 2D clusters and islands, and finally to 3D Li growth, and the consequent approach to the bulk Li value. The Li-Li bonding probably also causes depolarization of some of the Li-MgO bonding, which is supported by the aforementioned DFT calculations.[13] A Li_4 cluster on a terrace has much less downward charge transfer than a Li atom at a step. The Li atoms in Li_4 transfer charge instead to the volume between the four Li atoms (above a Mg ion), which does not lead to a downward dipole. Those calculations also include estimates of the work function changes associated with different periodic Li structures which are consistent with this picture and our measured trend with coverage. The work function reaches a minimum and starts to increase above 0.5 ML, which is just where the growth of Li switches from Li mainly populating MgO sites to Li mainly populating sites in the second and higher layers of 3D Li clusters. Thus, the increase in work function is associated with 3D Li growth and the simple approach to the value for bulk-like Li(solid).

D. Heat of adsorption: Li on pristine MgO(100)

Figure 5 shows the differential heat of adsorption of Li on pristine MgO(100) at 300 K as a function of Li coverage. This is actually a plot of the (negative) standard enthalpy of adsorption at 300 K, with the energy of the Li gas corrected to 300 K (see experimental section). The curve shows an average of four experimental runs. The pulse-to-pulse standard deviation at high Li coverages (where the heat of adsorption was constant) was 1.4 kJ/mol, and the experiment-to-experiment standard deviation was less than 9 kJ/mol (5.7%). In order to rule out possible effects on the heats of adsorption of surface damage by electrons (from doing AES after growth of the MgO(100) film), a calorimetric control experiment of Li adsorption on MgO(100) was performed, with the MgO film prepared in exactly the same way, but without doing AES or LEED. No significant difference was observed in the initial heat or the heat change versus the coverage.

The experiment-to-experiment standard deviation was observed to change with Li coverage. As mentioned, at high coverage (when the heat of adsorption was constant at the heat of sublimation) the standard deviation was <9 kJ/mol. However, at low-coverage (<0.4 ML) the standard deviation changed significantly (~30 kJ/mol in the first 0.1 ML, which decreased with coverage till above ~0.4 ML where it was constant again at <9 kJ/mol). It is likely that this was due to differences in the initial defect concentration on the MgO(100) film, since we observed a steady rise in the initial heat of adsorption by ~135 kJ/mol with the amount of Ar^+ ion dosage (see below).

On the pristine 4-nm-thick MgO(100) film, the heat of adsorption starts at 260 kJ/mol. By ~0.25 ML the heat of adsorption fell to 160 kJ/mol and reached a minimum of 153 kJ/mol by 0.4 ML. Following this, the heat increased slightly to the heat of sublimation of Li (159 kJ/mol, see Ref. 46) by ~1.5 ML.

These heat data for the 4 nm film have been analyzed in detail previously based on similar measurements of Ca adsorption energies on identically-prepared MgO(100) surfaces, and DFT calculations of the adsorption energies and migration barriers for both Li and Ca atoms and clusters on MgO(100) terrace and defect sites.[11] These data (as well as those for MgO surfaces with higher defect densities created by Ar-ion sputtering, see below) were semiquantitatively reproduced with a kinetic model described in detail in Ref. 11. In that model, the initially high heat of Li adsorption at low coverage was attributed to Li adatoms populating strong-binding intrinsic defect sites (mainly steps and kinks) and the simultaneous formation of some 2D Li clusters, starting at those defects but growing out onto the terraces. The intrinsic defects were estimated to have an average heat of adsorption of ~400 kJ/mol and the Li on terrace sites in 2D clusters or in small 3D clusters to have a heat of adsorption very near the bulk sublimation energy. The rapid decrease in the heat to a minimum was attributed to the saturation by Li of a low concentration of MgO defect sites which are intrinsic to the as-prepared MgO(100) thin film (which cover only 4% of the surface), and the consequent increase to 100% in the probability of populating terrace sites within 2D clusters or sites on top of 3D clusters. This model also required Li monomers on terraces to be highly mobile, consistent with DFT.[11]

The small rise in adsorption heat from this minimum to the heat of sublimation can be attributed to the formation of larger and larger 3D Li particles on the surface, a particle size effect whereby metal atoms in larger particles have greater stability, eventually reaching the bulk cohesive energy, as has been observed for other metals on the MgO(100) surface.[25,26]

E. Heat of adsorption at surface defects: Li on Ar^+ sputtered MgO(100)

We assume that the main intrinsic defects on the as-prepared MgO(100) surface are steps and kinks, since STM images of similarly-prepared MgO(100) thin films[16] show these defects to be common. Such sites are often nucleation centers for 2D and 3D metal clusters on MgO(100).[47,48] Point defects on MgO(100) surfaces also have been found to act as nucleation centers of metal particles.[21,49–53] The defects include O vacancies on terraces, Mg vacancies, and MgO divacancies. The most common of these defects is thought to be O vacancies, although previous studies have found that their concentration is tiny (less than a few percent of a ML) using our preparation technique,[21,54] and that they mainly exist at step edges.[54,55]

To confirm the effect of MgO(100) surface defects on the heat of Li adsorption, we created extra defects by lightly sputtering the pristine MgO(100) surface at 300 K with Ar^+ ions (1000 eV). Experiments studying the impact of argon ion bombardment of MgO(100) have shown that the surface stoichiometry does not change during bombardment,[56–58] and that the dominant structural unit removed from the oxide surface was clusters of MgO, leaving divacancy clusters on the surface.[59] Other studies done using electron-energy-loss spectroscopy on sputter-damaged MgO(100) films showed that band-gap states produced by sputtering could be "healed" by oxygen dosing, but this study did not rule out other type of defect formation from sputtering.[60]

Our studies of the heats of adsorption of Ca on pristine and sputter-damaged MgO(100) surfaces prepared in the same way showed that the initial heat of adsorption of Ca did not change with the extent of sputtering.[11,12] Combined with DFT calculations which showed that Ca is very mobile except when trapped at defects, but immobile at defects, this led us to conclude that the defect types and their ratios of concentrations did not change much with sputtering.[11] Thus, even on the sputter-damaged surface, the main defects are assumed to be similar to steps and kinks, consistent with the observation of MgO clusters as the dominant species removed by sputtering (see above).

Figure 6 shows the heat versus Li coverage for the pristine 4-nm-thick MgO(100) film (closed circles) along with two experiments with different amounts of Ar^+ dosed to identically prepared films: a low dose ($\sim 1\times 10^{14}$ Ar^+ ions/cm^2) and a high dose ($\sim 7\times 10^{14}$ Ar^+ ions/cm^2). We mention that these estimates of the magnitude of the ion doses are very crude both here and in our paper about Ca adsorption.[11,12] This is because these ion currents were measured without biasing the sample to prevent escape of low-energy electrons and with the ion beam irradiating not only the MgO but also a much larger area of sample holder whose surface was not cleaned. Thus, the secondary electron emission yields could have been very different from case to case, easily causing relative errors greater than threefold. On the low ion dosed films, the initial heat of adsorption was 315 kJ/mol, ~50 kJ/mol above the pristine surface value. The higher ion dose yielded an even higher initial heat of adsorption, 400 kJ/mol.

Both ion doses in Fig. 6 gave substantially higher heats of adsorption than pristine MgO(100) at all Li coverages below

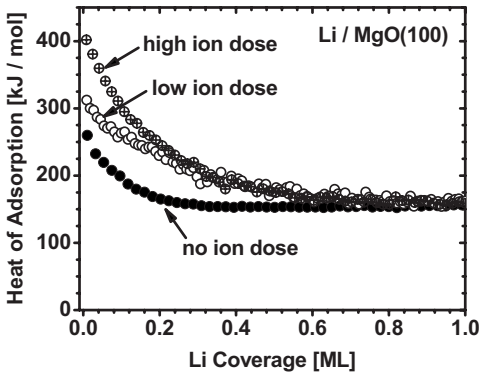

FIG. 6. The heat of adsorption versus Li coverage at room temperature; on (●) pristine 4-nm-thick MgO(100), (○) a film irradiated with a small Ar^+ ion dose, and (⊕) a film irradiated with a larger Ar^+ ion dose.

~0.7 ML. This is the same coverage range where Li is adsorbing mainly in the first layer (see above). These sputter induced increases in heat of adsorption are attributed to more Li atoms adsorbing at defect sites. The continual increase in the initial heat of adsorption with increasing ion doses implies that not all Li atoms are adsorbing at defect sites in the first pulse; therefore, some Li atoms are trapped in adsorption sites that keep them from reaching the more favorable defect adsorption sites. Based on DFT calculations, we can attribute these "trap" sites to the edges of 2D Li islands nucleated at steps and kinks.[11] A difference between Li and Ca adsorption is that these same sites do not trap Ca adatoms, which quickly move from them at 300 K.[11] Sputtered films also took longer to approach the bulk heat of sublimation than pristine MgO(100), 0.25 ML versus 0.8 ML for sputtered films.

The same DFT-based kinetic model described above that fit the heat data for the pristine surface was also able to semiquantitatively reproduce these heat data for the sputtered surfaces as well.[11] The fraction of surface sites that are defects was a parameter in that model, and found to be 14% for the less-sputtered surface and 22% for the more-sputtered surface, compared to 4% for the pristine MgO(100). That model is also consistent with the ISS data above.[11]

F. Effect of MgO(100) film thickness on Li heat of adsorption

As shown by the gray circles on Fig. 5, the 1 nm MgO(100) films had a higher initial heat of adsorption for Li than the 4 nm MgO(100) films (315 vs 260 kJ/mol), and took much longer to reach the heat of sublimation (1.5 versus 0.25 ML).

Two possible reasons for the difference between 1 and 4 nm MgO(100) films are that 1 nm films might have more intrinsic defects than 4 nm films, or that 1 nm films allow electronic interactions to occur between the Li adsorbate and the underlying Mo support that are not allowed for the 4 nm MgO. Recent STM work on MgO(100) thin films grown on Mo(100)[14–18] have shown that 7 ML (1.5 nm) films have similar morphology and defect density as 18 ML (3.8 nm) MgO(100) films. Thus, we expect that that our 1 and 4 nm

films have similar defect types and densities. We should point out that 2 ML (0.4 nm) MgO(100) films on Mo(100) show quite different appearance in STM,[14,16,17] but differences are expected to arise when approaching so near to the 1 ML limit.

Although theoretical calculations have shown that films of 3–4 ML (~1 nm) thickness have electronic properties almost identical to bulk MgO(100),[55,61,62] both experimental and theoretical investigations have shown that the binding of adsorbates on 2–4 ML MgO(100) films can be different than these same adsorbates on bulk MgO(100) or very thick MgO(100) films, depending on the nature of the underlying metal substrate.[63–65] The explanation provided by theory is that tunneling of electrons occurs from or to the underlying metal, through the thin oxide film, either from or to the adsorbate.[45,63,66] Depending on the work function of the underlying metal and the electronic properties of the adsorbate, electron transfer can become energetically favorable for some metal substrates but not others. For example, DFT calculations[45] show that K binds weakly to a free-standing MgO(100) slab (~14 kJ/mol), but much more strongly to an ultrathin (2 ML) MgO(100) layer supported on Ag(100) (~40 kJ/mol), where it donates charge to the underlying Ag substrate. It may be that a similar effect is operating here, whereby electron transfer from the Li to the underlying Mo is energetically feasible at a certain coverage, but kinetically allowed by tunneling only through the thin (1 nm) MgO spacer, but not through the 4 nm spacer.

IV. CONCLUSIONS

Lithium adsorbs on MgO(100) at defect sites (mainly steps and kinks and analogous sites at screw dislocations) with a heat of adsorption as high as 410 kJ/mol. The binding at these defects is rather cationic, with electron transfer to nearby oxygen atoms and a large work function decrease. As the Li coverage grows, Li makes 2D islands which nucleate at step edges and grow out onto the terraces. The Li in these 2D islands is still partially cationic, but much less so, and it binds much less strongly to the MgO (~160 kJ/mol). There is a kinetic competition between Li finding defects and Li getting trapped at terrace sites on the edges of these islands, with the latter becoming more rapid as the coverage grows. Sputtering the MgO with Ar^+ ions leads to more defects and a higher probability that these stronger-bonding defects sites populate at low coverage. Recent DFT calculations support these results and predict stronger electron transfer from Li to the MgO when at steps and kinks than at terraces, and decreasing charge transfer as 2D Li clusters grow. The film morphology as probed by AES and ISS evolves with increasing Li coverage in the way expected if Li gas atoms which impinge onto existing Li islands stay on top of Li islands, but Li atoms which impinge on free MgO sites stay attached to MgO (i.e., cannot down step or up step).

ACKNOWLEDGMENTS

The authors would like to acknowledge the Department of Energy, Office of Basic Energy Sciences, Chemical Sciences Division Grant Number DE-FG02-96ER14630, for support of this work. J.A.F. would like to acknowledge the Center for Nanotechnology at the UW for an NSF-supported IGERT Award (DGE-0504573). We thank Lijun Xu and Graeme Henkelman for providing a draft of their unpublished paper and for many insightful and enjoyable discussions.

*Corresponding author. FAX: +1 206 685-4305; campbell@chem.washington.edu

[1] J. H. Lunsford, Angew. Chem. Int. Ed. Engl. **34**, 970 (1995).
[2] Y. Kuo, F. Behrendt, and M. Lerch, Z. Phys. Chem. **221**, 1017 (2007).
[3] L. Leveles, K. Seshan, J. A. Lercher, and L. Lefferts, J. Catal. **218**, 296 (2003).
[4] T. Kendelewicz, P. Liu, G. E. Brown, E. J. Nelson, and P. Pianetta, Surf. Sci. **352-354**, 451 (1996).
[5] M. Brause, D. Ochs, J. Gunster, T. Mayer, B. Braun, V. Puchin, W. Maus-Friedrichs, and V. Kempter, Surf. Sci. **383**, 216 (1997).
[6] H. H. Huang, X. Jiang, Z. Zou, W. S. Chin, G. Q. Xu, W. L. Dai, K. N. Fan, and J. F. Deng, Surf. Sci. **412-413**, 555 (1998).
[7] J. A. Snyder, J. E. Jaffe, M. Gutowski, Z. Lin, and A. C. Hess, J. Chem. Phys. **112**, 3014 (2000).
[8] E. Giamello, D. Murphy, L. Ravera, S. Coluccia, and A. Zecchina, J. Chem. Soc., Faraday Trans. **90**, 3167 (1994).
[9] S. Brazzelli, C. Di Valentin, G. Pacchioni, E. Giamello, and M. Chiesa, J. Phys. Chem. B **107**, 8498 (2003).
[10] J. C. Lian, E. Finazzi, C. Di Valentin, T. Risse, H.-J. Gao, G. Pacchioni, and H.-J. Freund, Chem. Phys. Lett. **450**, 308 (2008).
[11] J. A. Farmer, C. T. Campbell, L. Xu, and G. Henkelman, J. Am. Chem. Soc. **131**, 3098 (2009).
[12] J. F. Zhu, J. A. Farmer, N. Ruzycki, L. Xu, C. T. Campbell, and G. Henkelman, J. Am. Chem. Soc. **130**, 2314 (2008).
[13] L. Xu and G. Henkelman (unpublished).
[14] S. Benedetti, P. Torelli, S. Valeri, H. M. Benia, N. Nilius, and G. Renaud, Phys. Rev. B **78**, 195411 (2008).
[15] H. M. Benia, P. Myrach, and N. Nilius, New J. Phys. **10**, 013010 (2008).
[16] S. Benedetti, H. M. Benia, N. Nilius, S. Valeri, and H.-J. Freund, Chem. Phys. Lett. **430**, 330 (2006).
[17] M. C. Gallagher, M. S. Fyfield, L. A. Bumm, J. P. Cowin, and S. A. Joyce, Thin Solid Films **445**, 90 (2003).
[18] M. C. Gallagher, M. S. Fyfield, J. P. Cowin, and S. A. Joyce, Surf. Sci. **339**, L909 (1995).
[19] M.-C. Wu, C. M. Truong, and D. W. Goodman, Phys. Rev. B **46**, 12688 (1992).
[20] Y. D. Kim, J. Stultz, and D. W. Goodman, Surf. Sci. **506**, 228 (2002).
[21] Y. D. Kim, J. Stultz, T. Wei, and D. W. Goodman, J. Phys. Chem. B **106**, 6827 (2002).
[22] J. T. Stuckless, N. A. Frei, and C. T. Campbell, Rev. Sci. Instrum. **69**, 2427 (1998).
[23] S. F. Diaz, J. F. Zhu, N. Shamir, and C. T. Campbell, Sens.

Actuators B **107**, 454 (2005).
[24] S. W. Pauls and C. T. Campbell, Surf. Sci. **226**, 250 (1990).
[25] D. E. Starr, D. J. Bald, J. E. Musgrove, J. T. Ranney, and C. T. Campbell, J. Chem. Phys. **114**, 3752 (2001).
[26] J. H. Larsen, J. T. Ranney, D. E. Starr, J. E. Musgrove, and C. T. Campbell, Phys. Rev. B **63**, 195410 (2001).
[27] R. Memeo, F. Ciccacci, C. Mariani, and S. Ossicini, Thin Solid Films **109**, 159 (1983).
[28] M.-G. Barthes and A. Rolland, Thin Solid Films **76**, 45 (1981).
[29] S. Berge, P. O. Gartland, and B. J. Slagsvold, Surf. Sci. **43**, 275 (1974).
[30] H. Nakane, S. Satoh, and H. Adachi, J. Vac. Sci. Technol. B **23**, 769 (2005).
[31] J. C. Riviere, *Work Function: Measurements and Results*, edited by M. Green (Dekker, New York, 1969), Vol. 1, p. 179.
[32] J. Gunster, G. Liu, V. Kempter, and D. W. Goodman, Surf. Sci. **415**, 303 (1998).
[33] L. N. Kantorovich, A. L. Shluger, P. V. Sushko, J. Gunster, P. Stracke, D. W. Goodman, and V. Kempter, Faraday Discuss. **114**, 173 (1999).
[34] J. R. Stevenson and E. B. Hensley, J. Appl. Phys. **32**, 166 (1961).
[35] V. E. Henrich and P. A. Cox, *The Surface Science of Metal Oxides* (Cambridge University Press, Cambridge/New York, 1996), p. 461.
[36] C. Weindel, H. J. Jänsch, G. Kirchner, H. Kleine, J. J. Paggel, J. Roth, H. Winnefeld, and D. Fick, Phys. Rev. B **71**, 115318 (2005).
[37] C. Bromberger, H. J. Jänsch, and D. Fick, Surf. Sci. **506**, 129 (2002).
[38] Y. B. Losovyj, N. T. Dubyk, and F. M. Gonchar, Vacuum **50**, 85 (1998).
[39] V. K. Medvedev, A. G. Naumovets, and T. P. Smereka, Surf. Sci. **34**, 368 (1973).
[40] P. A. Anderson, Phys. Rev. **75**, 1205 (1949).
[41] A. P. Ovchinnikov and B. M. Tsarev, Sov. Phys. Solid State **9**, 2766 (1968).
[42] V. K. Medvedev and T. P. Smereka, Sov. Phys. Solid State **16**, 1599 (1974).
[43] C. T. Campbell, Annu. Rev. Phys. Chem. **41**, 775 (1990).
[44] D. Murphy, E. Giamello, and A. Zecchina, J. Phys. Chem. **97**, 1739 (1993).
[45] L. Giordano and G. Pacchioni, Phys. Chem. Chem. Phys. **8**, 3335 (2006).
[46] J. G. Speight, *Lange's Handbook of Chemistry*, 16th ed. (McGraw-Hill, NY, 2005).
[47] C. T. Campbell, J. Chem. Soc., Faraday Trans. **92**, 1435 (1996).
[48] C. Duriez, C. Chapon, C. R. Henry, and J. M. Rickard, Surf. Sci. **230**, 123 (1990).
[49] A. Bogicevic and D. R. Jennison, Surf. Sci. **515**, L481 (2002).
[50] M. Sterrer, M. Yulikov, E. Fischbach, M. Heyde, H.-P. Rust, G. Pacchioni, T. Risse, and H.-J. Freund, Angew. Chem., Int. Ed. **45**, 2630 (2006).
[51] D. Fuks, Y. F. Zhukovskii, E. A. Kotomin, and D. E. Ellis, Surf. Sci. **600**, L99 (2006).
[52] A. V. Matveev, K. M. Neyman, I. V. Yudanov, and N. Rosch, Surf. Sci. **426**, 123 (1999).
[53] L. Xu, G. Henkelman, C. T. Campbell, and H. Jonsson, Surf. Sci. **600**, 1351 (2006).
[54] M. Sterrer, E. Fischbach, T. Risse, and H.-J. Freund, Phys. Rev. Lett. **94**, 186101 (2005).
[55] J. Carrasco, N. Lopez, F. Illas, and H.-J. Freund, J. Chem. Phys. **125**, 074711 (2006).
[56] V. S. Smentkowski, Prog. Surf. Sci. **64**, 1 (2000).
[57] I. Bertoti, R. Kelly, M. Mohai, and A. Toth, Surf. Interface Anal. **19**, 291 (1992).
[58] G. Marietta, F. Iacona, and R. Kelly, Nucl. Instrum. Methods Phys. Res. B **65**, 97 (1992).
[59] J. B. Malherbe, S. Hofmann, and J. M. Sanz, Appl. Surf. Sci. **27**, 355 (1986).
[60] D. Peterka, C. Tegenkamp, K.-M. Schroder, W. Ernst, and H. Pfnur, Surf. Sci. **431**, 146 (1999).
[61] S. Schintke, S. Messerli, M. Pivetta, F. Patthey, L. Libioulle, M. Stengel, A. De Vita, and W.-D. Schneider, Phys. Rev. Lett. **87**, 276801 (2001).
[62] L. Giordano, M. Baistrocchi, and G. Pacchioni, Phys. Rev. B **72**, 115403 (2005).
[63] D. Ricci, A. Bongiorno, G. Pacchioni, and U. Landman, Phys. Rev. Lett. **97**, 036106 (2006).
[64] M. Sterrer, T. Risse, M. Heyde, H.-P. Rust, and H.-J. Freund, Phys. Rev. Lett. **98**, 206103 (2007).
[65] D. E. Starr, C. Weis, S. Yamamoto, A. Nilsson, and H. Bluhm, J. Phys. Chem. C **113**, 7355 (2009).
[66] G. Pacchioni, L. Giordano, and M. Baistrocchi, Phys. Rev. Lett. **94**, 226104 (2005).
[67] M. P. Seah and W. A. Dench, Surf. Interface Anal. **1**, 2 (1979).